Analysis of Conversion Efficiency and Capacity Reduction in Electrical Storage Facilities by Peak Shift Control of Bifacial Photovoltaics.

Shin'ya Obara
Kitami Institute of Technology, Power Engineering Lab., Dep. of Electrical and Electronic Engineering
Koen-cho 165, Kitami, Hokkaido 090-8507, Japan
obara@mail.kitami-it.ac.jp
phone/FAX +81-157-26-9262

Daisuke Konno
Kitami Institute of Technology, Power Engineering Lab., Dep. of Electrical and Electronic Engineering
Koen-cho 165, Kitami, Hokkaido 090-8507, Japan

Yuta Utsugi
Kitami Institute of Technology, Power Engineering Lab., Dep. of Electrical and Electronic Engineering
Koen-cho 165, Kitami, Hokkaido 090-8507, Japan

Jorge Morel
Kitami Institute of Technology, Power Engineering Lab., Dep. of Electrical and Electronic Engineering
Koen-cho 165, Kitami, Hokkaido 090-8507, Japan

Abstract

Bifacial photovoltaics are widely investigated with the aim of reducing the amount of silicon used and increasing conversion efficiencies. The conversion efficiency of bifacial photovoltaics depends on the quantity of solar radiation incident on the reverse face. Furthermore, controlling the orientation can distribute the times of peak power output in the morning and afternoon to better match the demand. In this study, the demand patterns of individual houses or the whole Hokkaido region were analyzed assuming the substitution of a conventional large-scale electric power system with one using bifacial photovoltaics. The supply–demand balances and electrical storage capacities were investigated. When comparing a large scale solar power plant (mega-solar power plant) using monofacial photovoltaics or vertical bifacial photovoltaics (in which the orientation could be adjusted), the supply–demand could be better balanced for individual houses in the latter case, thereby allowing the storage capacity to be reduced. A bifacial solar module was modeled by 3D-CAD (three dimensional computer aided design) and thermal fluid analysis. The module temperature distribution of bifacial photovoltaics was calculated with respect to the environmental conditions (wind flow, direct and diffuse solar radiation, etc) and

internal heat generation, as well as the orientation of the solar panels. Furthermore, the conversion efficiency of bifacial photovoltaics can be easily obtained from the analysis result of modular temperature distribution and the relation between temperature and conversion efficiency.

Key Words : Bifacial photovoltaics, Conversion efficiency, Photovoltaic power station, Heat transfer analysis.

1. Introduction

There are examples of study on evaluating the reliability of large-scale photovoltaic (PV) systems and the effect of photovoltaics interconnection on the reliability of local distribution system [1-3]. Furthermore, cost and efficiency of new design photovoltaics are investigated [4, 5]. Bifacial photovoltaics are being investigated for the purpose of reducing the quantities of silicon required and increasing the conversion efficiency [6-8]. The amount of silicon can be reduced by reducing the distance that the charge carriers need to travel in a bifacial photovoltaic system. Standard monofacial solar cells have an opaque backing on the reverse face, whereas bifacial photovoltaics have a transparent glass on the back that allows the input of solar radiation—which is the source of electricity generation—from the reverse face also. Moreover, when solar radiation is incident on the reverse face, the dependence of the electric power generation on the orientation and angle of inclination of bifacial photovoltaics is small compared to standard monofacial photovoltaics. The reverse face of a bifacial photovoltaic system can easily capture reflected and diffused solar radiation, and therefore, these systems are thought to be suitable for installation on, for example, the roofs of parking areas, walls of buildings, fences, and rooftop signs [9-11]. The conversion efficiency of bifacial photovoltaics greatly depends on the amount of incident solar radiation on the reverse face. Moreover, when exposed to high temperature, the conversion efficiency falls, as for the standard solar cells [12]. Therefore, in order to predict the electric power generation of bifacial photovoltaics, thermal fluid analysis can be applied to obtain the temperature distribution in the module as a function of the environmental conditions (outside air temperature, vector of the wind, solar position, direct solar radiation, diffuse solar radiation, radiation reflected from the ground) and geometrical parameters related to the installation (orientation, number of modules, height from the ground, etc.). The conversion efficiency can be obtained by applying the relation between module temperature and conversion efficiency to the temperature distribution of the bifacial photovoltaics obtained from thermal fluid analysis. A simple method for obtaining the conversion efficiency from such analysis is proposed here.

It is necessary to compensate the inconsistent power output of photovoltaics by connecting them with a commercial power system. However, in order to make the power output of photovoltaics increase with an electrical power system, a stable supply from the photovoltaic power plant side is desired. Electrical

storage equipment is required for stabilizing the supply from a large-scale photovoltaic power plant (mega-solar power station), and although NAS cells (Na–S batteries), pumped hydro power generation, etc. can be considered, they are very expensive. An alternative for controlling the peaks in power-generation output is by changing the orientation of vertical bifacial photovoltaics, as will be presented in this study. When installing bifacial photovoltaics in the east–west directions, peaks occur in the electric power generation in the morning and the afternoon. On the other hand, two load peaks are seen in the general electricity demand in the morning and evening, and hence, if the two output peaks of bifacial photovoltaic generation and the two load peaks of electricity demand can be synchronized, it may be possible to reduce the storage capacity for balancing the supply–demand. This could result in a reduction in the installation cost of electrical storage equipment. In this study, the supply–demand balance and storage capacity facilities of a mega-solar power plant using bifacial photovoltaics is investigated on the basis of the load pattern of individual houses and assuming substitution of a large-scale electric power system.

2. Materials and Methods

2.1 Scheme of Bifacial Photovoltaics

Figure 1 shows a schematic of a bifacial photovoltaic device in which the active n-type single crystal layer is sandwiched between two amorphous silicon layers (above and below), forming a symmetrical cell. Therefore, electricity is generated when light enters from either the upper or lower face of a bifacial solar cell. However, because the intensity of the incident light is not equal on both sides, the amount of electrical power generation is not simply doubled. Moreover, because the maximum voltage (open circuit voltage) falls when the temperature of a solar cell rises, the output power will drop under high-temperature conditions. Although there are few voltage drops due to the amorphous material under high temperatures compared to the single crystal, the temperature characteristics of bifacial photovoltaics are slightly better than single crystal silicon because of the resistances of other components.

2.2 Output Characteristics of Bifacial Photovoltaics

Figure 2 shows the output characteristics of bifacial photovoltaics obtained during testing. Figure 2 (a) shows the relationship between the voltage and the current of bifacial photovoltaics in the case where there is no input of solar radiation to the reverse face. Moreover, Fig. 2 (b) shows the output characteristics of the bifacial photovoltaics based on Fig. 2 (a). The maximum conversion efficiency in Fig. 2 (b) is approximately 16% at 25 ℃. On the other hand, Fig. 2 (c) shows the relationship between the power-generation output and the conversion efficiency of bifacial photovoltaics with solar radiation of 1.0 kW/m^2 incident on the front face, showing that the conversion efficiency significantly changes depending on the magnitude of the radiation incident on the reverse face. In order to maintain a high

conversion efficiency of bifacial photovoltaics, it is necessary to ensure that the incident insolation on the reverse face is at least 30% of that on the front surface. Therefore, because there is little input of solar radiation to the reverse face, even if bifacial photovoltaics are installed as monofacial photovoltaics, a high conversion efficiency is not obtained. Figure 2 (d) shows the temperature characteristics of the conversion efficiency when a solar radiation of 1.0 kW/m^2 enters the front face of a bifacial photovoltaic as a function of the ratio of solar radiation incident on the reverse face to the front face.

2.3 Large-scale solar power system (mega-solar power plant)

Figure 3 (a) shows the case of a large-scale photovoltaic power plant currently installed in Japan, which has monofacial photovoltaic cells facing south with 45° angle of inclination from horizontal. For comparison, Fig. 3 (b) shows the proposed system with vertical bifacial photovoltaics in the east–west directions. Figure 4 (a) shows the output characteristics of each module of the monofacial photovoltaics facing south, as shown in Fig. 3 (a), and the bifacial photovoltaics for east–west, as shown in Fig. 3 (b). However, the normal power of the monofacial photovoltaics in Fig. 4 (a) is smaller than that for the bifacial photovoltaics. Although the maximum output of the monofacial photovoltaics facing south is obtained during noon, the peak output of the bifacial photovoltaics installed in the east–west directions is obtained in the morning and afternoon. As the next section will describe, when the orientation of vertical bifacial photovoltaics is changed, the magnitude of the output peaks obtained in the morning and afternoon can be adjusted. Therefore, the capacity of the electrical storage facilities required to compensate for the difference in power generation between the mega-solar power system and the power demand may be reduced by controlling the orientation of vertical bifacial photovoltaics on the basis of the load pattern.

Figure 4 (b) shows output characteristics when combining the monofacial photovoltaics and bifacial photovoltaics described in Figs. 3 (a) and (b) (green curve). The supply-and-demand difference over the course of the day can be minimized by choosing an appropriate ratio of monofacial and bifacial photovoltaic cells and by optimizing the orientation of the bifacial photovoltaics on the basis of load estimations.

2.4 Outline of Proposed System

Figure 5 shows the system configuration of a mega-solar power plant using vertical bifacial photovoltaics considered in this study. The DC output of the vertical bifacial photovoltaics can supply electric power to a grid from high-voltage equipment and a transformer through a DC–DC converter and an inverter (from Path A-1 to A-3 in Fig. 5). Alternatively, the DC output of the vertical bifacial photovoltaics can be supplied to the demand side through the inverter (Path A-1, B-4). Furthermore, the DC output of the vertical bifacial photovoltaics can also be stored in a battery through the DC–DC

converter and the inverter (Path B-1). After the electric power stored in the battery passes through the DC–DC converter and the inverter, the electric current is divided—Path B-2, B-3, and A-2 for supplying the power grid and Path B-2, B-3, and B-4 for supplying the demand side.

Any fluctuations in the output of bifacial photovoltaics have a serious influence on the stability of the power supply. Therefore, the output of a mega-solar power plant is stabilized by storing the electricity or by connecting it to a commercial (conventional) power system. As shown in Fig. 5, storage using a pumped-storage hydroelectric power plant and NAS batteries is considered in the mega-solar power plant assumed in this study.

2.5 System Operation

Figure 6 shows the output power as a function of time of day for the mega-solar power plant operating with vertical bifacial photovoltaics, as shown in Figure 6 (a), or monofacial photovoltaics, as shown in Fig. 6 (b), and their charge–discharge operations. In both cases the surplus power stored is supplied from the electrical storage equipment when the demand exceeds generation. It can be seen that the maximum in supply–demand is smaller for the mega-solar power plant with bifacial photovoltaics compared to that for the plant with the monofacial photovoltaics. Moreover, because the output pattern of the bifacial photovoltaics more closely resembles the load characteristics than that of the monofacial photovoltaics, many small time zones of the supply–demand difference may appear. Therefore, the mega-solar power plant using bifacial photovoltaics can expect a reduction in the amount of charges and discharges compared to conventional monofacial photovoltaics.

3. Theory

3.1 Heat flow analysis and conversion efficiency

Although the temperature of a module rises owing to the internal generation of heat and the solar radiation incident on the bifacial photovoltaics, the module can be cooled by the wind. Therefore, the temperature distribution of the solar module is analyzed by calculating its energy balance. Figure 7 shows a schematic of the energy and fluid fluxes relevant for a bifacial photovoltaic module. The direct solar radiation $q_{sd,t}$, diffuse solar radiation $q_{sf,t}$, and quantity-of-heat $q_{ca,t}$ from the flow of open air over the bifacial photovoltaic module and the direct-current-power $q_{dc,t}$ are determined over the sampling time t. Moreover, the generation of heat of $q_{gh,t}$ occurs as a result of the electrical resistance of the module. Heat ($q_{ca,t}$) is removed by heat transfer between the front face of the module and open air. Furthermore, corresponding to the difference between the module surface temperature $T_{pm,t}$ and the outside air temperature $T_{\infty,t}$, the heat $q_{rb,t}$ is removed by radiative heat transfer. The front face of a solar module is covered with a special glass, and in general, the reflected solar energy $q_{r,t}$ from the glass surface is less than 1%. The temperature $T_{pm,t}$ of the solar module is determined from the energy

balance of all these components. All radiation energies containing $q_{rb,t}$ and q_{sf}, which are reflected from the ground and incident on the reverse face of bifacial photovoltaics, are analyzed by the ray tracing method. The conversion efficiency of the bifacial photovoltaic module will be obtained from the model characteristics shown in Fig. 2 (d). When $T_{pm,t}$ and $q_{rb,t}$ are fixed, Eq. (1) describes the energy balance of the radiation t enters the solar module in a sampling time t, where

$$q_{sd,j,t} + q_{sf,j,t} = q_{dc,t} + q_{gh,t} = R_{Load,t} \cdot I_{pm,t}^2 + R_{ir,t} \cdot I_{pm,t}^2 \quad (1)$$

The input of direct solar radiation $q_{sd,j,t}$ and diffuse solar radiation $q_{sf,j,t}$ to the surface of j is outputted as Joule's heat $q_{gh,t}$ by DC output $q_{dc,t}$ corresponding to load $R_{Load,t}$ of the solar cell and internal resistance $R_{ir,t}$ of the solar module.

3.2 Heat Transfer Analysis

3.2.1 Radiative Heat Transfer Analysis

(1) Radiation between surfaces

The radiation energy $q_{rT,out,j,t}$ emitted from the surface of j at the sampling time t is the sum of the emission (the first term of the right hand side) by surface j according to the Stefan–Boltzmann law and the reflected component (the second term of the right hand side) of the radiation energy emitted from surface j from surface i. Therefore, $q_{rT,out,j,t}$ is defined by Eq. (2).

$$q_{rT,out,j,t} = \varepsilon_j \cdot \sigma \cdot T_{j,t}^4 + \rho_{T,j} \cdot q_{rT,in,i,t} \quad (2)$$

Here ε_i, σ, $T_{j,t}$, and $\rho_{T,j}$ are emissivity, Stefan–Boltzmann constant, temperature of the surface, and reflectivity, respectively, while $q_{rT,in,i,t}$ is the heat radiation that enters into i in sampling time t.

(2) Direct solar radiation and diffuse solar radiation

Equation (3) describes the emission $q_{rS,out,j,t}$ of the radiation energy from surface j by input of direct solar radiation and diffuse solar radiation. Component $q_{sd,in,k,t}$ of the direct solar radiation enters surface j from an emission surface k of direct solar radiation, and component $q_{sf,in,l,t}$ of the diffuse solar radiation enters surface j from emission surface l of diffuse solar radiation. $q_{rS,out,j,t}$ is calculated by multiplying the sum of $q_{sd,in,k,t}$ and $q_{sf,in,l,t}$ by the reflectivity $\rho_{S,j}$ of the surface of j. The diffuse solar radiation $q_{sf,in,l,t}$ uniformly enters from all angles, and the magnitude of diffuse solar radiation is dependent on the weather.

$$q_{rS,out,j,t} = \rho_{S,j} \cdot \left(q_{sd,in,k,t} + q_{sf,in,l,t}\right) \quad (3)$$

(3) Net radiation

Equation (4) describes the total radiation energies emitted from surface j. In this study, the difference between the radiation energy emitted from surface j and the radiation energy which reaches j is defined as the net radiation $q_{rN,j,t}$, and is calculated using Eq. (5).

$$q_{r,out,j,t} = q_{rT,out,j,t} + q_{rS,out,j,t} \tag{4}$$

$$q_{rN,j,t} = q_{r,out,j,t} - q_{r,in,j,t} = \left(q_{rT,out,j,t} + q_{rS,out,j,t}\right) - \left(q_{rT,in,j,t} + q_{rS,in,j,t}\right) \tag{5}$$

The amount of energy exchange $Q_{rT,j,t}$ on the surface j is a function of the heat radiation $q_{rT,out,k,t}$ from surface k and the view factor (proportion of energy emitted from surface k that is incident on surface j), as shown by Eq. (6). Moreover, the amount of energy exchange $Q_{rS,j,t}$ by solar radiation on surface j is obtained from Eq. (7) by using direct solar radiation $q_{sd,in,k,t}$, diffuse solar radiation $q_{sf,in,l,t}$, and the radiation view factor $F_{j-k,t}$.

$$Q_{rT,j,t} = \sum_{k} F_{j-k,t} \cdot q_{rT,out,k,t} \tag{6}$$

$$Q_{rS,j,t} = \sum_{k} F_{j-k,t} \cdot q_{sd,in,k,t} + \sum_{l} F_{j-l,t} \cdot q_{sf,in,l,t} \tag{7}$$

Equations (8) and (9) are radiation energy equations using the radiative view factor for heat radiation and solar radiation. The radiation energy (heat radiation and solar radiation) input to the surface is calculable by introducing reflectivity $\rho_{T,j}$ from surface j, emissivity ε_j, surface temperature $T_{j,t}$, view factor $F_{j-k,t}$ between the surface of k and the surface of j, and radiation energy $q_{rT,j-k,t}$, $q_{rS,j-k,t}$, which enters from the surface of k, into Eqs. (8) and (9). The radiation view factor is calculated by the ray tracing method. Photons that simulate radiation energies are regularly emitted from the light source surface in the ray tracing model and a radiation view factor is determined from the number of photons arriving on the target surface.

$$q_{rT,in,j,t} - \rho_{T,j} \cdot \sum_{k} \left(F_{j-k,t} \cdot q_{rT,j-k,t}\right) = \varepsilon_j \cdot \sigma \cdot T_{j,t}^4 \tag{8}$$

$$q_{rS,in,j,t} - \rho_{S,j} \cdot \sum_{k} \left(F_{j-k,t} \cdot q_{rS,j-k,t}\right) = 0 \tag{9}$$

3.2.2 Temperature of Bifacial Photovoltaics Module

The temperature change $\left(T_{pm,t}-T_{pm,t-1}\right)$ of the solar module over sampling times $t-1$ to t is obtained using Eq. (10), where $Q_{ca,t}$, $Q_{gh,t}$, $Q_{ht,t}$, $Q_{r,t}$, and $Q_{tr,t}$ can be calculated by using Eq. (11)–Eq. (15), respectively, where the temperature of the solar module $T_{pm,t}$ can be found by inputting these values into Eq. (10). When the temperature $T_{pm,j,t}$ of the surface of j is obtained, the conversion efficiency can be calculated from the temperature characteristics of the bifacial photovoltaics—as shown in Fig. 2 (d). The amount of insolation entering the reverse face of bifacial photovoltaics gives the sum total of the reflected light from the ground and diffuse solar radiation.

$$Q_{ca,t}+Q_{gh,t}=G_{pm}\cdot c_{p,pm}\cdot\left(T_{pm,t}-T_{pm,t-1}\right)+Q_{ht,t}+Q_{r,t}+Q_{tr,t} \tag{10}$$

$$Q_{ca,t}=\rho_{\infty,t}\cdot c_{p,\infty,t}\cdot\left(T_{\infty,t}-T_{pm,t}\right)\cdot u_{\infty,t} \tag{11}$$

$$Q_{gh,t}=R_{ir}\cdot I_{pm,t}^{2} \tag{12}$$

$$Q_{ht,t}=A_{pm}\cdot h_{pm,t}\cdot\left(T_{pm.t}-T_{\infty,t}\right) \tag{13}$$

$$Q_{r,t}=\gamma_{r}\cdot\left(q_{sd,t}+q_{sf,t}\right) \tag{14}$$

$$Q_{tr,t}=\sigma\cdot A_{pm}\cdot\left(T_{pm,t}^{4}-T_{\infty,t}^{4}\right) \tag{15}$$

4. Analysis Flow and Analysis Conditions

4.1 Supply–Demand Balance of Mega-Solar Power Plant and Capacity of Electrical Storage Facilities

4.1.1 Analysis Conditions

(1) Object of investigation

The supply–demand requirements for matching specific power load patterns (individual houses or the whole Hokkaido region) using mega-solar power plant with vertical bifacial photovoltaics is clarified in this study, and the required electrical storage capacity is investigated. Because the output patterns of vertical bifacial photovoltaics depend on their orientation, the relationship between the orientation and storage capacity is discussed. Here we assume the case of a mega-solar power plant with bifacial photovoltaics installed at Kitami and investigate the representative days of the maximum and minimum power generation during 2012, which on the basis of the meteorological data [13], were on March 19 and November 26, respectively.

(2) Load pattern of individual houses

Figure 8 shows the load pattern of the individual houses used in the analysis, where power consumption by household appliances and electric lights is included but cooling and heating loads are not considered. As a result, large variations are not seen throughout the year in the load characteristics. The power output pattern of a 1000 m^2 area of bifacial photovoltaics is shown for both 60° and 90° angles of orientation on March 19, 2012 in Fig. 8. As shown in Fig. 9, the clockwise angle defines the orientation from the south; therefore, for example, 90° (thick blue line of bifacial photovoltaics data shown in Fig. 8) of the acceptance surface is oriented in the east–west direction. On the other hand, when the orientation of bifacial photovoltaics is 60° (thick red line as shown in Fig. 8), the height of the peak in the morning and the afternoon changes.

(3) Load pattern of whole Hokkaido region

Figure 10 shows the power load pattern of the whole Hokkaido region in 2010 [14]. Hokkaido is a wide area including Kitami with a population of 5,450,000 and land area of 83,456 km^2. The grid of 8,317 km is distributed over the area of Hokkaido, operated by the Hokkaido Electric Power Co., Inc. Electric power is supplied by 54 hydroelectric power stations (1.2 GW), 12 thermoelectric power plants (4.2 GW), one nuclear power station (2.1 GW), one natural steam power station (25 MW), and one photovoltaic power plant (1 MW). The pumped hydroelectric output is 1.0 GW over three sites (one under construction). The analysis in this study considers neither losses from the electrical power grid nor the capacity of the actual power transmission line.

(4) Analysis flow

Electric power generation of the mega-solar power plant for each sampling time is calculated by using recorded insolation data for each representation day (March 19 and November 26, 2012) at Kitami (lat. 43° 47'N and long. 143° 54'E). The maximum supply–demand difference on each day in accordance with the operation method shown in Fig. 6 was investigated by using the electric power generation as described in upper part and the load patterns of Fig. 8 and Fig. 10 . This maximum supply–demand difference was used to determine the electrical storage capacity.

4.2 Wind Analysis of Kitami Area and Analysis of Conversion Efficiency

Flow Simulation 2012 was used to analyze a 3D-CAD (three dimensional computer aided design) model of the photovoltaic system prepared by SolidWorks® regarding the net radiation, heat transfer rate $h_{pm,j,t}$, and temperature $T_{pm,j,t}$ of surface j. The internal resistance of the monofacial side and bifacial photovoltaics was 1.0 Ω/m^2, and the maximum conversion efficiency and temperature coefficient of monofacial photovoltaics was set to 18% and 0.4%/℃, respectively. Laminar flow of fluid and turbulence was used for the Navier–Stokes equation, and the transport equation ($k-\varepsilon$ model) was applied to turbulence kinetic energy [15] in the calculation of the streamline of space surrounding the solar power generators. After clarifying the module temperature distribution as described in Section 3.1,

the conversion efficiency of the bifacial photovoltaics was obtained from the relationship between the temperature of the module shown in Fig. 2 (d) and the conversion efficiency. It was necessary to provide meteorological data (outside air temperature, solar radiation, wind direction, and wind speed) for simulating the operating environment of the photovoltaics and physical properties of the solids and fluids in the analysis. The meteorological data used for analysis was sourced from the Meteorological Agency [13], Japan Weather Association [16], and New Energy and Industrial Technology Development Organization (NEDO) [17].

5. Results

5.1 Analysis Conditions

The maximum conversion efficiency of the modular output terminal was set to 20%, assuming single-crystal-silicon-type monofacial photovoltaics. The output characteristics of the bifacial photovoltaics are given in Fig. 2. The monofacial and bifacial photovoltaics were installed 1 m above the ground, and the internal resistance of a solar module was set to 1.0 Ω/m^2. The circumference of a solar module is surrounded with air, and the reflectivity (scatter reflection) of the ground was set to 0.2. Physical properties of the silicon were applied to the model of a solar module, and the location was set to Kitami. The wind speed, direction of the wind, solar position, outside air temperature, etc. of the neighborhood were arbitrarily given according to the location.

5.2 Supply–Demand Balance and Storage Capacity

5.2.1 Output Characteristics of Vertical Solar Cells

Figures 11 and 12 show the outputs of March 19 and November 26 of vertical monofacial photovoltaics and vertical bifacial photovoltaics, respectively. The monofacial photovoltaics were installed with a southerly orientation (0° angle of direction), with the angles of inclination of the bifacial photovoltaics set at 0°, 30°, 60°, 90°, 120° and 150°. The difference in the outputs from the two representative days of maximum (March 19) or minimum (November 26) electric power generation is very large, as shown in Fig. 11 and Fig. 12. Moreover, the characteristics of the power-generation peaks in the morning and afternoon greatly depend on the orientation of the vertical bifacial photovoltaics.

The electrical power outputs (Figs. 12 (b)–(f)) of the vertical bifacial photovoltaics with 30° or higher angles of direction are approximately 4% lower than the total generation (Fig. 11 (a)) on March 19 with the vertical monofacial photovoltaics facing south. It is thought that this drop in the output with angles of direction other than 0° is due to the difference between the direct solar radiation and the radiative view factor of the acceptance surface as well as the difference in the maximum conversion efficiency of the bifacial photovoltaics and monofacial photovoltaics. The electrical storage capacities at the time of

introducing each output pattern of Figs. 12 (a)–(f) into the load patterns shown in Figs. 8 and 10 are determined as follows.

5.2.2 Supply–Demand Balance and Storage Capacity Based on Load Patterns of Individual Houses.

Figures 13 and 14 show the supply–demand balances and the storage capacities at the time of introducing into the load pattern of individual houses the mega-solar power plant with vertical monofacial photovoltaics or vertical bifacial photovoltaics. The results for March 19 (maximum power generation) are compared in Fig. 13 (a) (left side) and Fig. 14 (a) (left side). An area of 1000 m^2 of monofacial photovoltaics or bifacial photovoltaics can meet the electricity demands of 125–130 houses or 120–127 houses, respectively (namely the number of ridges which are balanced by the supply–demand). Because of distribution and storage losses, in reality, fewer houses will be able to be supplied. The reason bifacial photovoltaics provide for fewer houses than monofacial photovoltaics is the orientation given to the vertical bifacial photovoltaics; electric power generation will decrease rather than electric power generation of the monofacial photovoltaics facing south, and the maximum conversion efficiency of bifacial photovoltaics with little insolation incident on the reverse face is lower than for the monofacial photovoltaics, as described in Section 5.2.1. The power storage capacity for the supply–demand balance of the number of houses as described is 0.95 MWh from 0.86 MWh in the monofacial photovoltaics (facing south, with an angle of inclination of 40–90°) and 0.89 MWh from 0.8 MWh in the bifacial photovoltaics on March 19 (right figures of Figs. 13 (a) and 14 (a)). By adjusting the orientation of the vertical bifacial photovoltaics facing south (Fig. 12), a maximum reduction of 16% in the required storage capacity can be achieved for monofacial photovoltaics with an angle of inclination of 40–90°. Therefore, optimizing the orientation of vertical bifacial photovoltaics can significantly reduce the storage capacity required for a mega-solar power plant.

When the supply–demand balances for the load pattern of the individual houses on November 26 (minimum output) are compared (left sides of Figs. 13 (b) and Fig. 14 (b)), because there is little electric power generation output, the power demand cannot be satisfied without the use of stored power (surplus power from other days). When a mega-solar power plant is installed in Kitami, although the required storage capacity was calculated to be small for a day of maximum power generation, the day of minimum power generation requires much larger storage capacity, which attends to the demand for several days.

5.2.3 Supply–Demand Balance and Storage Capacity Based on Load Pattern Assuming Substitution of Large-Scale Electric Power System

Figures 15 and 16 show supply–demand balances and the storage capacities when the power load pattern for the mega-solar power plant (vertical monofacial or bifacial photovoltaics) is considered over the whole Hokkaido region. Figure 15 (a) shows the case of the monofacial photovoltaics facing south on

March 19. In order to supply the electric power for the whole Hokkaido region using vertical monofacial photovoltaics with an angle of inclination of 90° requires acceptance surface of 76 km^2 and an angle of inclination of 40° requires acceptance surface of 70 km^2. In addition, corresponding electrical storage equipments of 116 GWh and 97 GWh are required. On the other hand, Fig. 16 (a) shows the case of vertical bifacial photovoltaics for the same conditions. In order to supply the electric power of the whole Hokkaido region by using vertical bifacial photovoltaics, 0° (for north and south) orientation requires an acceptance surface of 76 km^2, and 150° requires 80 km^2 from angles of direction of 30°. Furthermore, it is not based on the orientation, but the electrical storage equipment of 108 GWh is required. The storage capacity in the case of applying the power load pattern of vertical bifacial photovoltaics over the whole Hokkaido region decreases when solar cells are facing south (0°). However, when different orientations are used, the storage capacity requirement increases compared to monofacial photovoltaics with an angle of inclination of 40°. Using the output characteristics of bifacial photovoltaics is not advantageous with the characteristics of the power load pattern in March representation day of the whole Hokkaido region shown in Fig. 8 (a).

When the supply–demand balance based on the load pattern of the whole Hokkaido region on November 26 is compared (left side of Figs. 15 (b) and 16 (b)), the power generation is low for all solar cells. As a result, using surplus power (stored from another day) or backup from another power source (e.g., external system or pumped hydro power generation) is required.

5.3 Conversion Efficiency of Bifacial Photovoltaics

Figure 17 shows an example of the temperature distribution results for the bifacial photovoltaics described in Section 4.2. In order to study the temperature rise in the solar cell, time durations of 12:00 and 14:00 on August 15 (mid-summer in Kitami) were investigated. The direct solar radiation and outside air temperature of this location will make the temperature of the module high during most of the year. Figures 17 (a) and (b) show the temperature distribution of the vertical bifacial photovoltaics of 90° (for east and west) orientation. 1 m/s weak wind (air temperature of 30 ℃) was flowing from southeast in Fig. 17 (a), and the windless condition is shown in Fig. 17 (b). The mean temperature of the modules shown in Figs. 17 (a) and (b) were 62 ℃ and 76 ℃, respectively, with conversion efficiencies of 16.8% and 16.0%, respectively (calculated from data shown in Fig. 2 (d)). It turned out that the conversion efficiency increased only 0.8% with a weak wind flow (Figs. 17 (a) and (b)). On the other hand, Fig. 17 (c) shows the results of the temperature distribution for 15° orientation of each bifacial photovoltaics shown in Figs. 17 (a) and (b). Because the modular mean temperature falls to 49 ℃, the conversion efficiency increased to 17.6%.

Figures 17 (d) and (e) shows examples of a 3 kW system, 12 sets of bifacial photovoltaic modules with a width of 0.940 m and length of 1.56 m. As shown in Fig. 17 (f), the systems described by Figs. 17 (d)

and (e) were examined on campus at the Kitami Institute of Technology in Japan. Owing to the windless condition, as shown in Fig. 17 (d), the modular mean temperature rises at 91 ℃ and the conversion efficiency falls to 14%. On the other hand, Fig. 17 (e) shows the case of wind flow of 3 m/s (at 30 ℃) flowing in from the southwest. Because the mean temperature of the module in this case is cooled to 55 ℃, the conversion efficiency increases to 17.3%. If the amount of insolation that enters the reverse face can be increased, as shown in Fig. 2 (d), the conversion efficiency of Figs. 17 (a)–(e) can be increased further. Therefore, it is easy to increase the input of reflected light from the ground into the reverse face by leveling a bifacial photovoltaic (Fig. 17 (g)). When 30% or more reflected insolation (relative to input into the front face) is input into the reverse face, as in the model of Fig. 17 (g), although the conversion efficiency should greatly increase, the conversion efficiency is only 14.8% (without wind) because the modular mean temperature rises to 100 ℃. When there is wind flow, it is expected that the conversion efficiency will significantly increase in the model of Fig. 17 (g).

6. Conclusions

Amorphous silicon bifacial photovoltaics were analyzed with respect to their supply–demand characteristics and modular conversion efficiency when operating in a mega-solar power plant. The following conclusions were obtained by numerical simulations.

(1) On the basis of the load pattern of individual houses or the whole Hokkaido region, assuming substitution of a large-scale electric power system, the supply–demand balance and storage capacity of a mega-solar power plant operating with bifacial photovoltaics were clarified. The storage capacity could be reduced by adjusting the orientation of vertical bifacial photovoltaics for the mega-solar power plant, which consists of monofacial photovoltaics in the load pattern of individual houses. However, no benefit of introducing bifacial photovoltaics was observed in the power load pattern when assuming substitution of the large-scale electric power system.

(2) Modeling of the solar module by using 3D-CAD and thermal fluid analysis, allowed module temperature distributions and conversion efficiencies to be calculated as a function of the given environmental conditions (e.g., wind flow) and geometry of the photovoltaics.

Acknowledgments

This work was partially undertaken in cooperation with PVG Solutions Inc., Kitami city, and the Hokkaido Government of 2012.

Nomenclature

A_{pm} : Area of a solar module [m^2]

$c_{p,pm}$: Specific heat of the solar module [J/(g·K)]

$c_{p,\infty}$: Specific heat of air [J/(g·K)]

F View factor

G_{pm} : Mass of the solar module [kg]

h_{pm} : Heat transfer rate on the surface of a solar module [kW/(m²·h·K)]

I_{pm} : Current of the solar cell [A]

Q_{ca} : Heat of air current [J]

q_{ca} : Rate of heat of air current [kW]

q_{dc} : Output rate of direct current [kW]

Q_{gh} : Heat of the solar module [J]

q_{gh} : Generation rate of heat of the solar module [kW]

Q_{ht} : Heat by heat transfer [J]

Q_r : Reflection energy of solar radiation [J]

q_r Reflection energy rate of solar radiation [kW]

q_{rb} Amount of insolation incident on the modules reverse face [kW]

q_{rN} Net radiation energy [kW]

Q_{rS} : Amount of radiation energy exchange by solar radiation [kW/m²]

q_{rS} : Solar radiation [kW/m²]

Q_{rT} : Amount of radiation energy exchange between two surfaces [kW/m²]

q_{rT} : Radiation energy between two surfaces [kW/m²]

q_{sd} : Direct solar radiation [kW/m²]

q_{sf} : Diffuse solar radiation [kW/m²]

Q_{tr} : Heat transfer of radiation [J]

q_{tr} : Heat transfer rate of radiation [kW]

R_{Load} : Resistance of load [Ω]

R_{ir} : Internal resistance [Ω]

T : Temperature [°C]

t : Sampling time [h]

T_{pm} : Surface temperature of solar module [°C]

T_∞ : Outside air temperature [°C]

u_∞ : Velocity of air [m/s]

Greek characters

ε : Emissivity

γ_r : Reflectivity of solar radiation on the surface of the solar module

ρ_S, ρ_T : Reflectivity

ρ_∞ : Density of air [kg/cm^3]

σ : Stefan–Boltzmann constant [J/(s·cm^2·K^4)]

References

[1] Zhanga P, Lia S, Wanga Y, Xiao W, Reliability assessment of photovoltaic power systems: Review of current status and future perspectives. Applied Energy 2013;104:822-833.

[2] Pavana M A, Mellitb A, Pierid De D, Kalogirou A S, A comparison between BNN and regression polynomial methods for the evaluation of the effect of soiling in large scale photovoltaic plants. Applied Energy 2013;108:392-401.

[3] Shah R, Mithulananthan N, Bansal C R, Damping performance analysis of battery energy storage system, ultracapacitor and shunt capacitor with large-scale photovoltaic plants. Applied Energy 2012;96:235-244.

[4] Su Y, Chan L C, Shu L, Tsui K L, Real-time prediction models for output power and efficiency of grid-connected solar photovoltaic systems, Applied Energy, 2012;93: 319-326.

[5] Sánchez R C, Milone H D, Buitrago H R, Simulation of photovoltaic centrals with dynamic shading Applied Energy 2013;103:278-289.

[6] Dwivedi N, Kumar S, Bisht A, Patel K, Sudhakar S, Simulation approach for optimization of device structure and thickness of HIT solar cells to achieve ~27% efficiency. Solar Energy 2013;88:31-41.

[7] Duran C, Deuser H, Harney R, Buck T, Approaches to an Improved IV and QE Characterization of Bifacial Silicon Solar Cells and the Prediction of their Module Performance. Energy Procedia 2011;8:88-93.

[8] Frank J, Rüdiger M, Fischer S, Goldschmidt J.C, Hermle M, Optical simulation of bifacial solar cells. Energy Procedia 2012;27:300-305.

[9] Panasonic Brings its HIT Double Solar Modules to the Global Market, Homepage of Panasonic Corporation, http://news.panasonic.net/archives/2012/0704_11168.html, 2013.

[10] Solar Energy, Homepage of Hitachi Ltd., http://www.hitachi.co.in/products/business/energy/solar_energy/, 2013.

[11] Homepage of Gamma Solar Corp., http://www.gammasolar.com/solar.asp?page_name=company, 2013.

[12] Teoa G H, Leeb S P, Hawladerb A M N, An active cooling system for photovoltaic modules. Applied Energy 2012;90:309-315.

[13] The past meteorological data, Information of the climatological statistics, Japan Meteorological Agency, http://www.data.jma.go.jp/obd/stats/etrn/ ;2013.

[14] Electricity status-of-use data in 2010, The past electricity status-of-use data, Hokkaido Electric

Power Co., Inc., http://denkiyoho.hepco.co.jp/download.html ;2013
[15] Technical Reference of the SolidWorks Flow Simulation 2012, Section 1, Dassault Systèmes SolidWorks Corporation, USA, 2012:3-14.
[16] tenki.jp, Japan Weather Association, http://tenki.jp/past/?month=1&year=2012 ;2013.
[17] Annual amount-of-insolation data base (METPV-11), New Energy and Industrial Technology Development Organization (NEDO), http://www.nedo.go.jp/library/nissharyou.html ;2013.

Captions

Fig. 1 Schematic showing the basic configuration of a bifacial solar cell.

Fig. 2 Output characteristics of a bifacial solar cell.
(a) Relationship between the voltage and current of a bifacial solar cell and the amount of insolation.
(b) Relationship between the voltage and wattage of a bifacial solar cell and the amount of insolation.
(c) Relationship between the input of solar radiation to the reverse face and total power output of the bifacial solar cell. Solar insolation 1.0 kW/m^2 on the front face.
(d) Temperature characteristics of the power-generation efficiency of a bifacial solar cell. Solar insolation 1.0 kW/m^2 on the front face.

Fig. 3 Mega-solar power station.
(a) Conventional system.
(b) Vertical installation of bifacial photovoltaics.

Fig. 4 Output characteristics of PV.
(a) Bifacial module.
(b) Hybrid bifacial and monofacial system.

Fig. 5 Proposed power generation and storage system.

Fig. 6 Model of electrical charge and discharge cycles of photovoltaic systems.
(a) Bifacial photovoltaics vertically installed.
(b) Monofacial photovoltaics installed with an optimal angle.

Fig. 7 Thermal model of a photovoltaic system.

Fig. 8 Relationship between the output of bifacial solar cell of 1000 m^2 and power consumption of various numbers of individual houses in March.

Fig. 9 Orientation.

Fig. 10 Electrical power supply of Hokkaido Electric Power Co. Inc. in 2010.
(a) From January to June.
(b) From August to December.

Fig. 11 Output characteristics of a monofacial PV facing south.
(a) 90° angle.
(b) 40° angle.

Fig. 12 Output characteristics of a vertical bifacial PV in Kitami.

Fig. 13 Supply–demand balance of monofacial PV power of 1000 m^2 based on the load pattern of individual houses.

Fig. 14 Supply–demand balance of vertical bifacial PV power of 1000 m^2 based on the load pattern of individual houses.

Fig. 15 Supply–demand balance of monofacial PV power of 1000 m^2 based on the supply pattern of the electric power company.

Fig. 16 Supply–demand balance of vertical bifacial PV power of 1000 m^2 based on the supply pattern of the electric power company.

Fig. 17 Results of thermal fluid analysis of bifacial PV on August 15 in Kitami (lat. 43°47′ N. and long. 143°54′ E).
(a) Orientation of 90° (facing east–west), 14:00, wind direction from the southeast of 1 m/s.
(b) Orientation of 90° (facing east–west), 14:00, no wind.
(c) Orientation of 15°, 14:00, wind direction from the southwest of 1 m/s.
(d) 0.940 m × 1.56 m bifacial modules of 12 sets, orientation of 0° (facing south), 14:00, no wind.
(e) 0.940 m × 1.56 m bifacial modules of 12 sets, the orientation of 0° (facing south), 12:00, wind direction from the southwest of 3 m/s.
(f) Photograph of 0.940 m × 1.56 m bifacial modules of 12 sets, orientation of 0°
(g) 0.940 m × 1.56 m bifacial modules of 12 sets, horizontal installation, 12:00, no wind.

Fig. 1 Schematic showing the basic configuration of a bifacial solar cell.

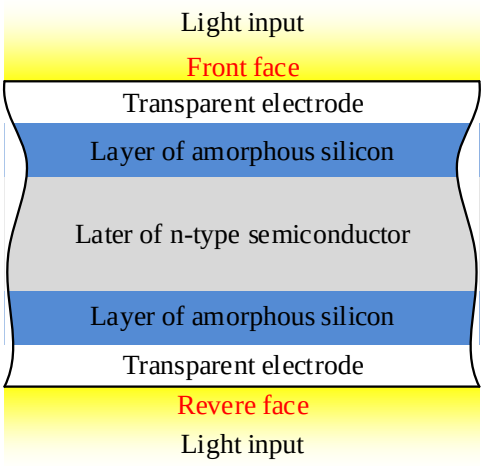

575 Fig. 2 Output characteristics of bifacial solar cells.

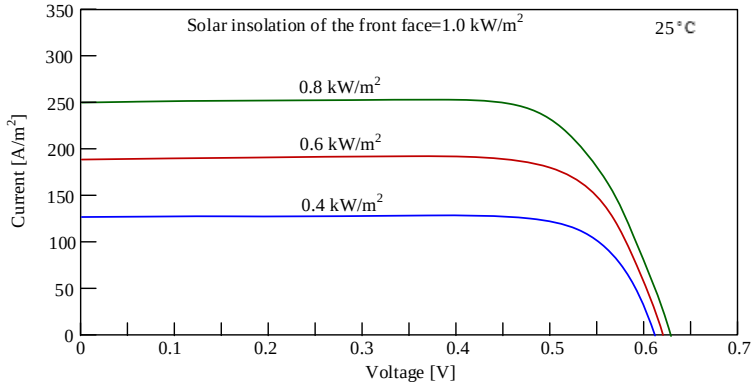

(a) Relationship between the voltage and current of a bifacial solar cell and the amount of insolation.

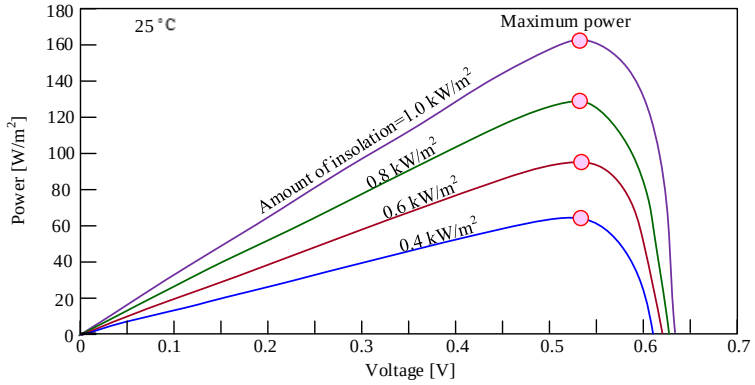

(b) Relationship between the voltage and wattage of a bifacial solar cell and the amount of insolation.

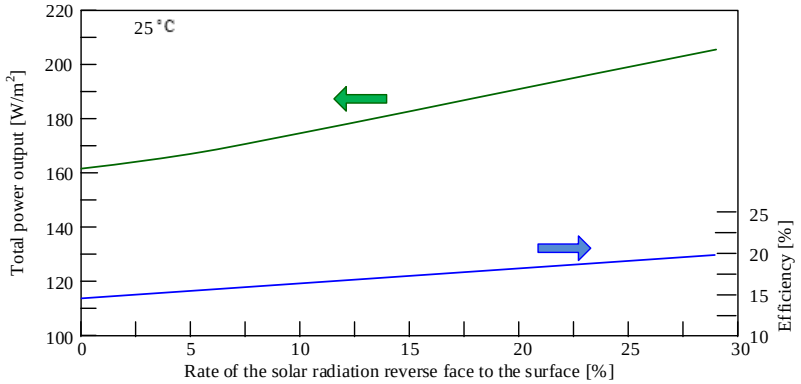

(c) Relationship between the input of solar radiation to the reverse face and total power output of the bifacial solar cell. Solar insolation 1.0 kW/m^2 on the front face.

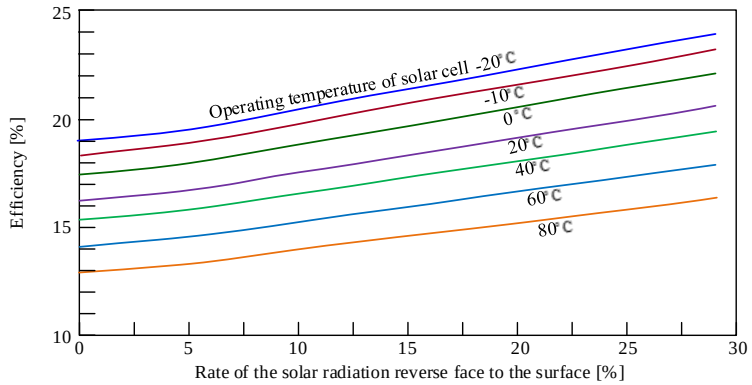

(d) Temperature characteristics of the power-generation efficiency of a bifacial solar cell. Solar insolation 1.0 kW/m^2 on the front face.

576 Fig. 3 Mega-solar power station.

577

578

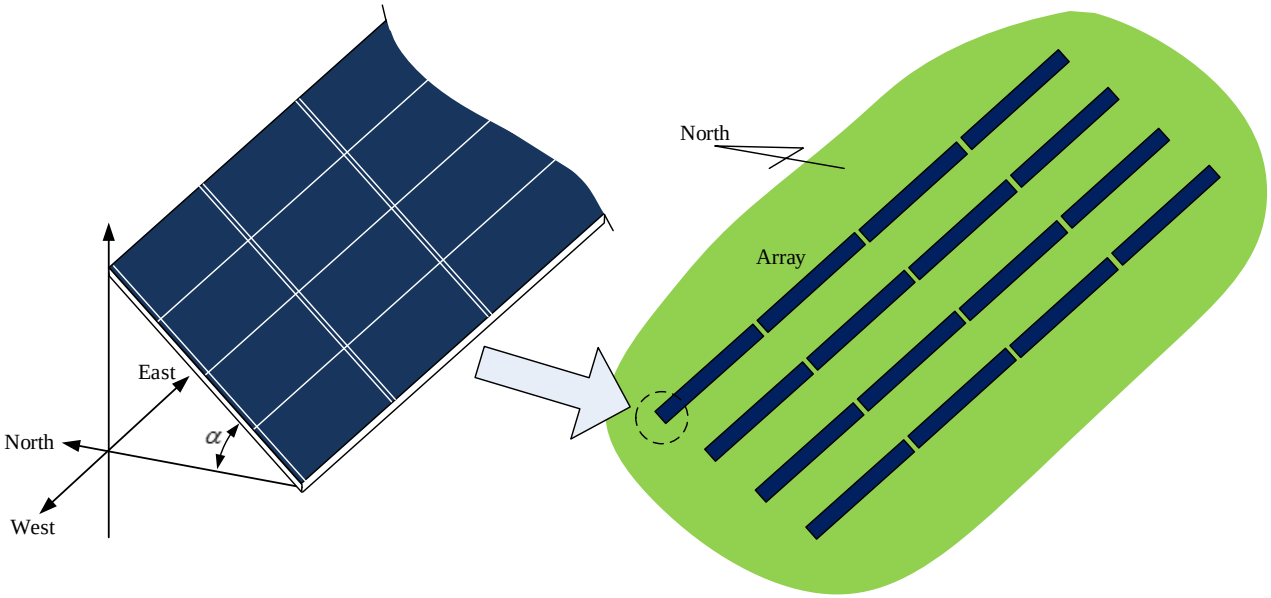

(a) Conventional system.

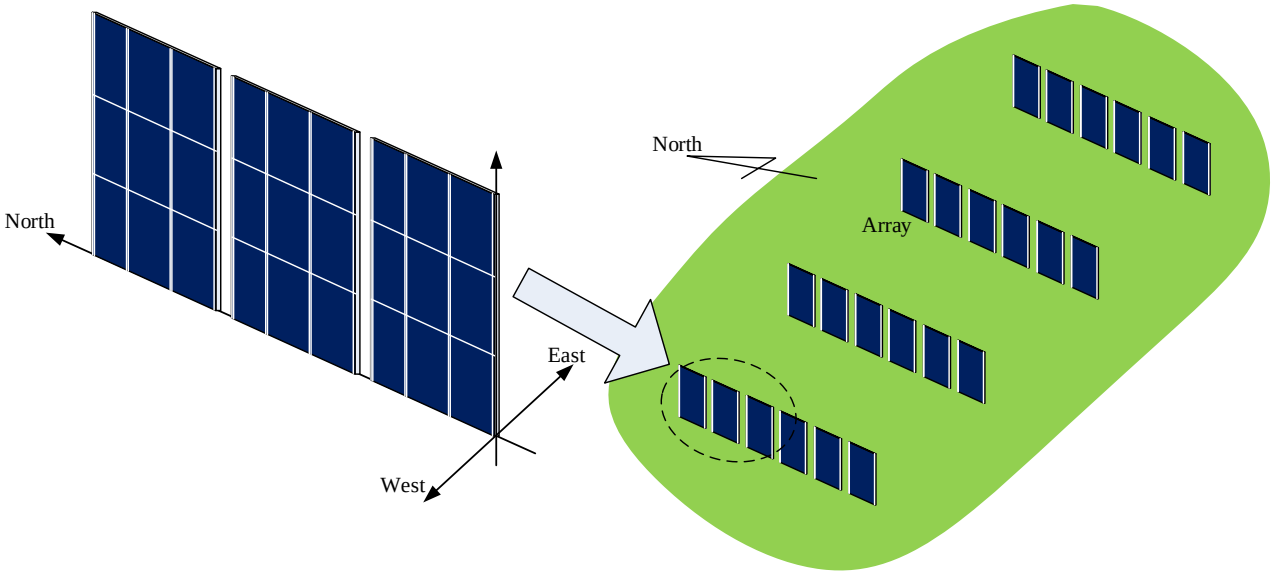

(b) Vertical installation of bifacial photovoltaics.

579

580

581

582

583

584 Fig. 4 Output characteristics of PV.

585

586

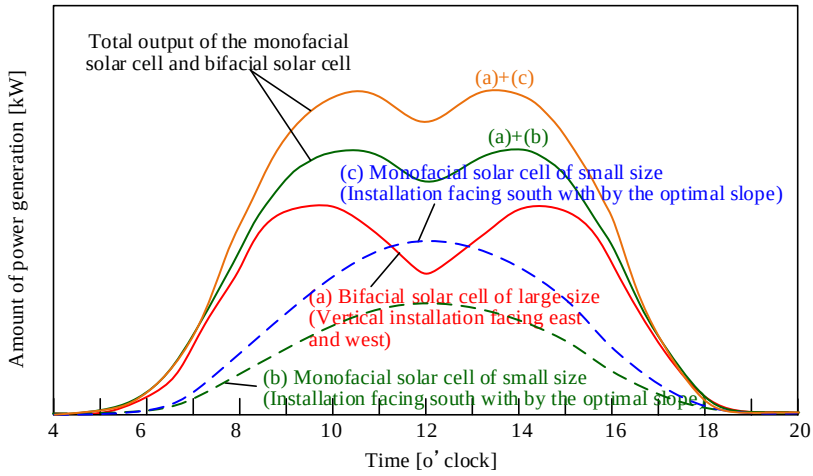

(a) Bifacial module.

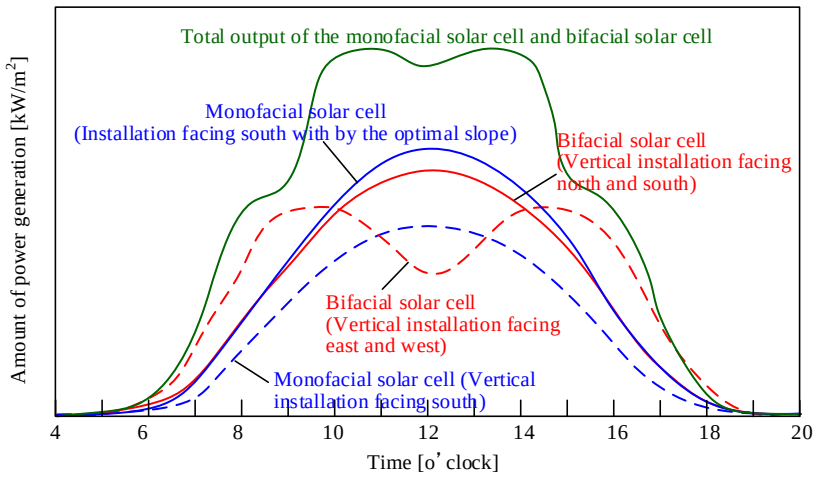

(b) Hybrid bifacial and monofacial system.

587

588

589

590

591

592

593

594

595

596

597

598 Fig. 5 Proposed power generation and storage system.

599

600

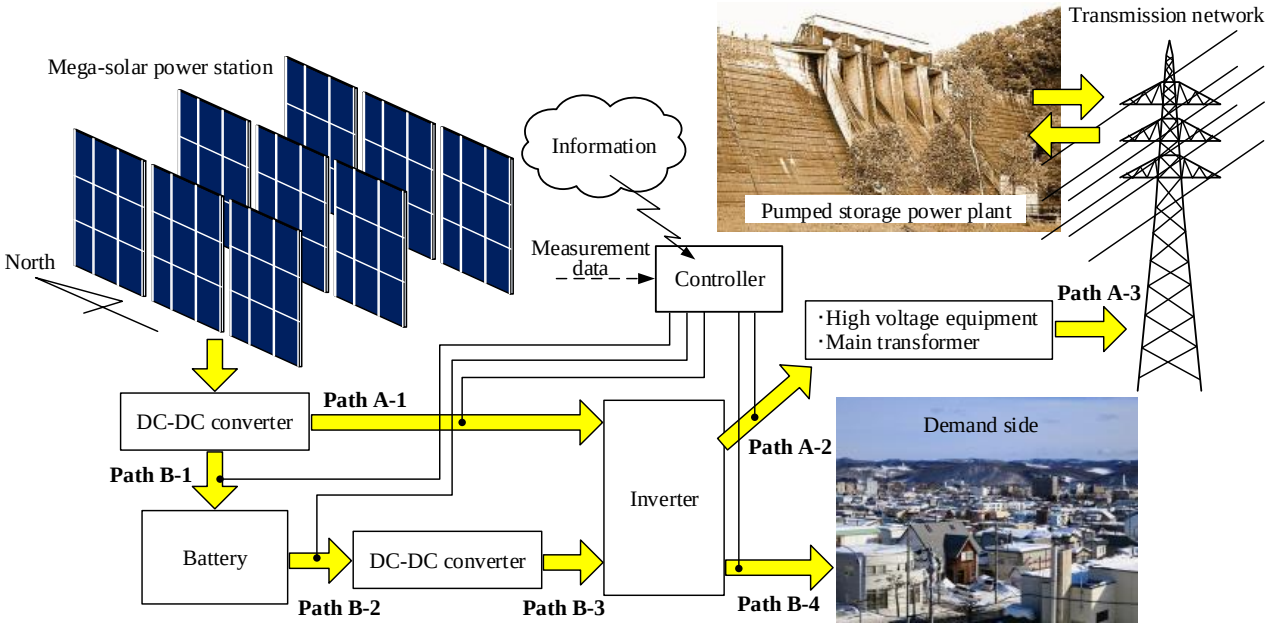

601

602

603

604

605

606

607

608

609

610

611

612

613

614

615

616

617

618

619

620 Fig. 6 Model of electrical charge and discharge cycles of photovoltaic systems.

621

622

623

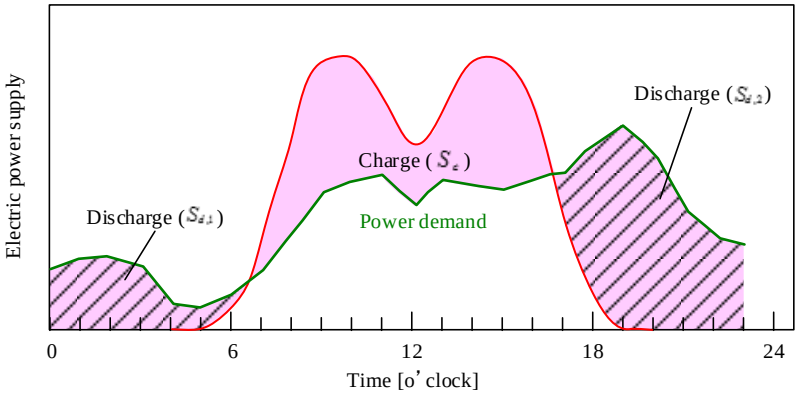

(a) Bifacial photovoltaics vertically installed.

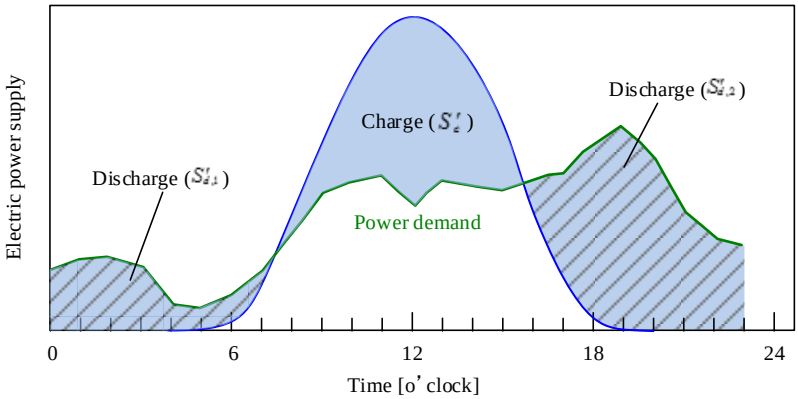

(b) Monofacial photovoltaics installed with an optimal angle.

624

625

626

627

628

629

630

631

632

633

634

635

636

637 Fig. 7 Thermal model of a photovoltaic system.

638

639

640

641

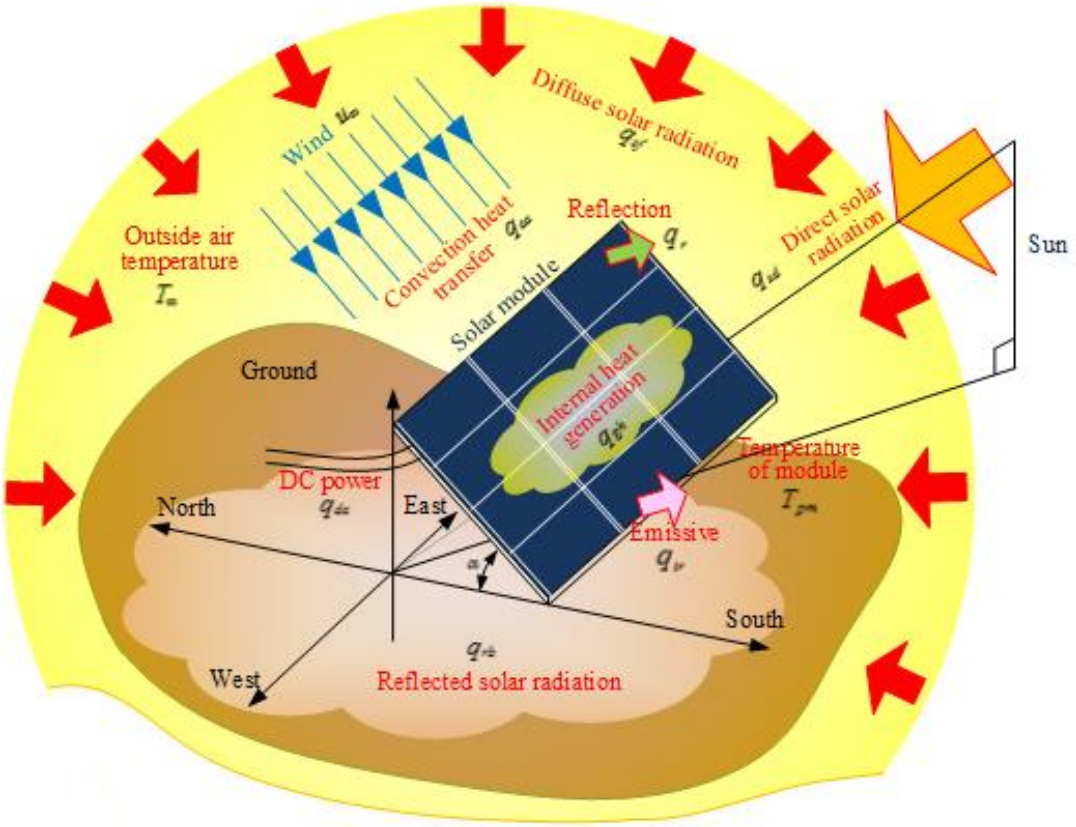

Fig. 7 Model of charge and discharge of electricity of photovoltaics

642

643

644

645

646

647

648

649

650

651

652

653 Fig. 8 Relationship between the output of a bifacial solar cell of 1000 m² and the power consumption
654 of various numbers of individual houses in March.
655
656
657
658

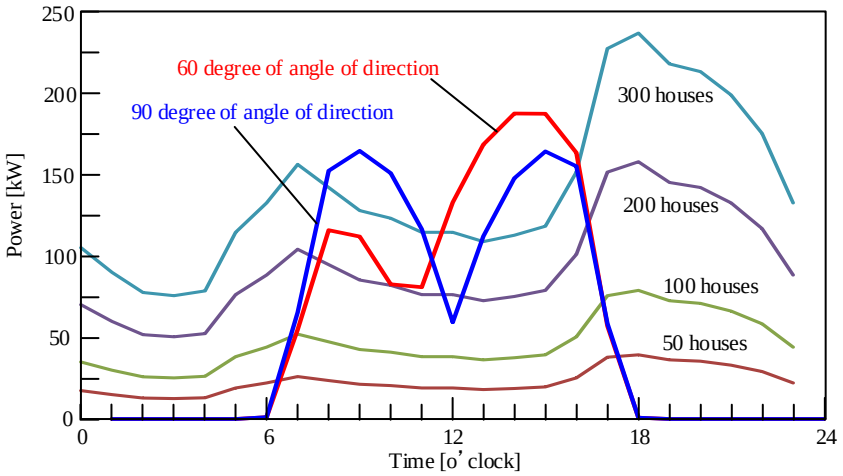

659
660
661
662
663 Fig. 9 Orientation
664
665

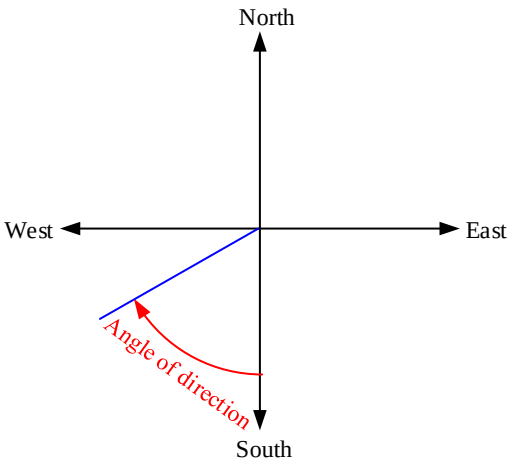

666
667
668

669 Fig. 10 Electric power supply of Hokkaido Electric Power Co. Inc. in 2010.

670

671

672

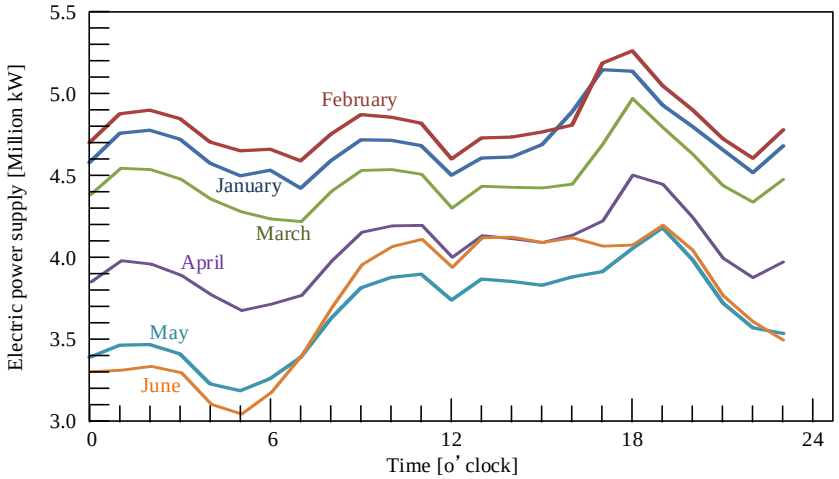

(a) From January to June.

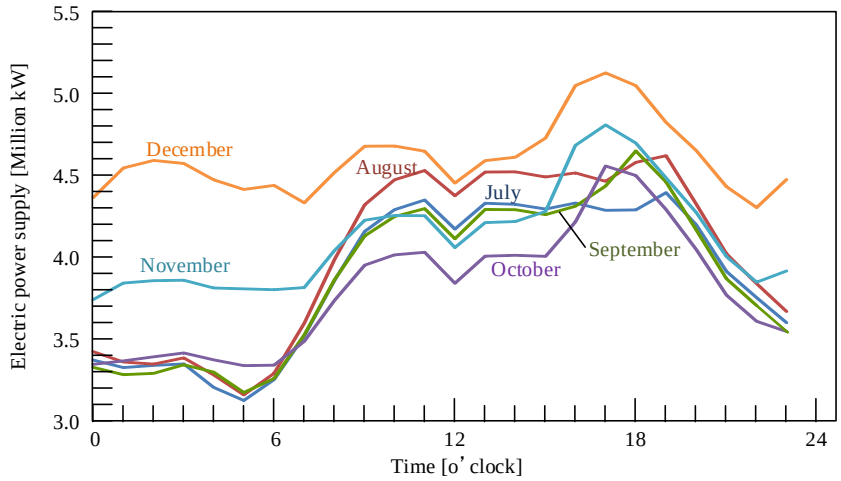

(b) From August to December.

673

674

675

676

677

678

679

680

681

682

683 Fig. 11 Output characteristics of monofacial PV facing south.

684

685

686

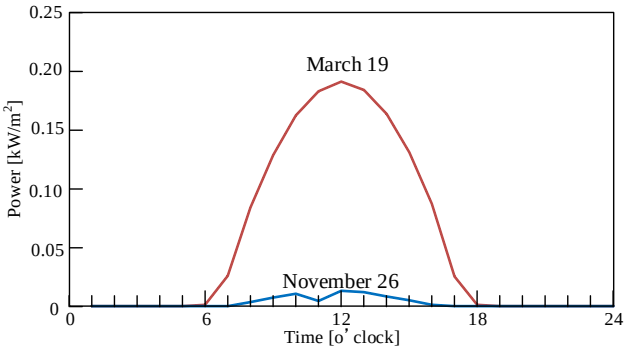

(a) 90° angle.

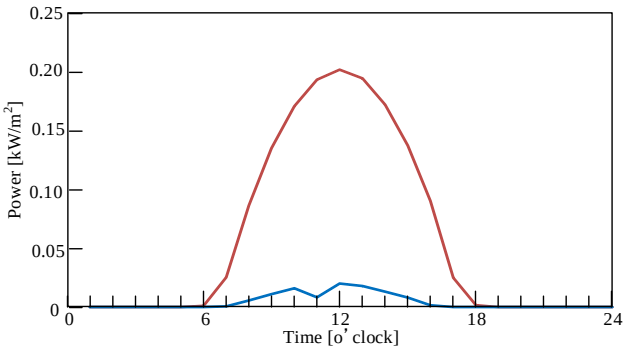

(b) 40° angle.

687

688

689

690

691

692

693

694

695

696

697

698

699

700

701

702

703

704

705

706

707

708

Fig. 12 Output characteristics of vertical bifacial PV in Kitami.

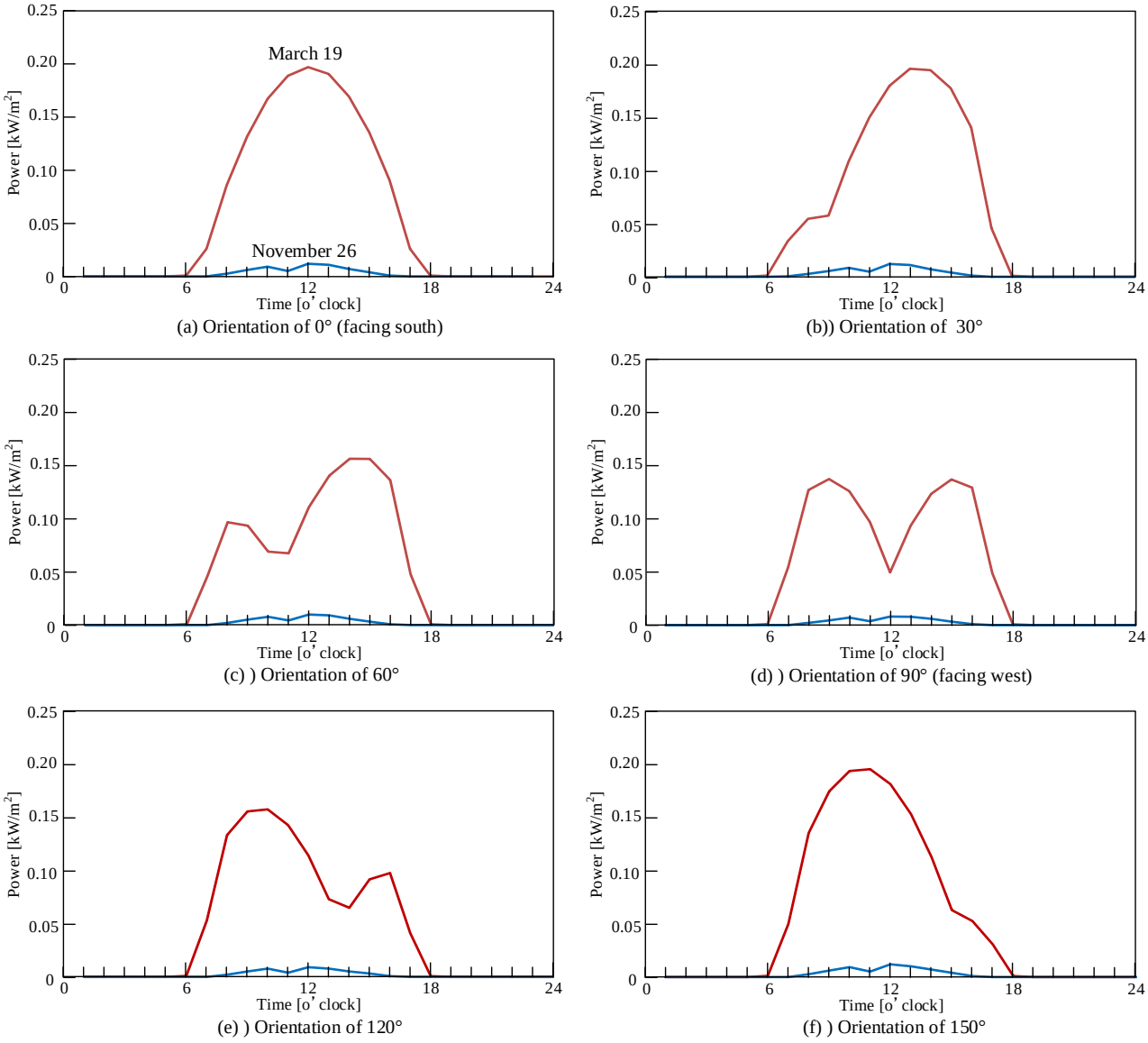

(a) Orientation of 0° (facing south)

(b)) Orientation of 30°

(c)) Orientation of 60°

(d)) Orientation of 90° (facing west)

(e)) Orientation of 120°

(f)) Orientation of 150°

721 Fig. 13 Supply-and-demand balance of monofacial PV power of 1000 m² based on the load pattern of
722 individual houses.
723
724
725

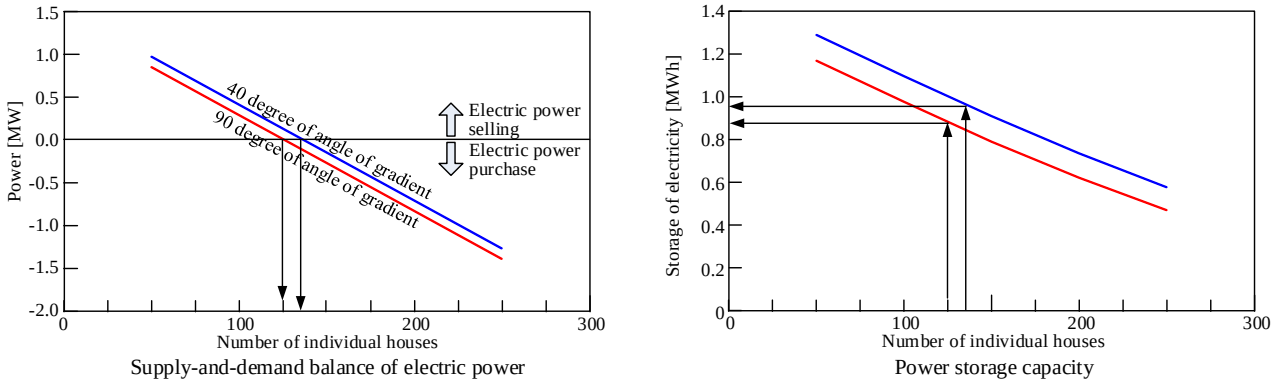

(a) March 19

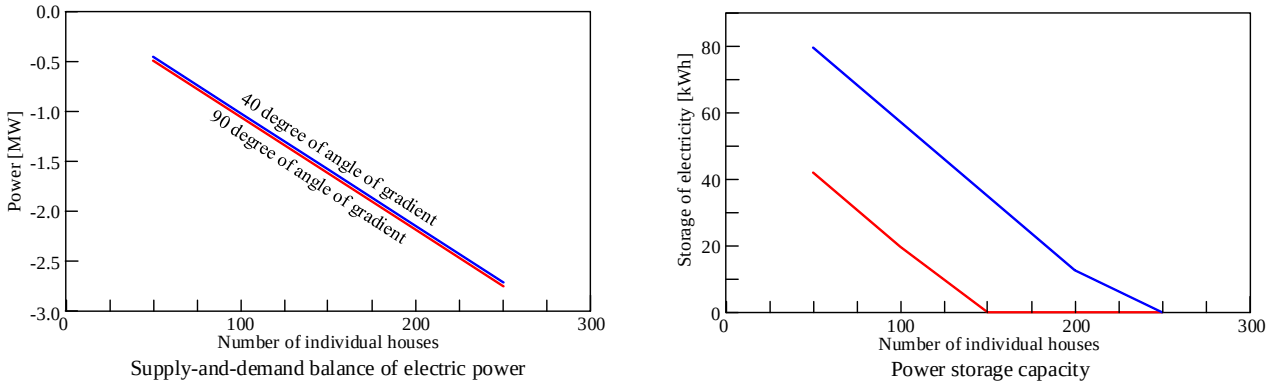

(b) November 26

726
727
728
729
730
731
732
733
734
735
736
737
738

Fig. 14 Supply-and-demand balance of vertical bifacial PV power of 1000 m² based on the load pattern of individual houses.

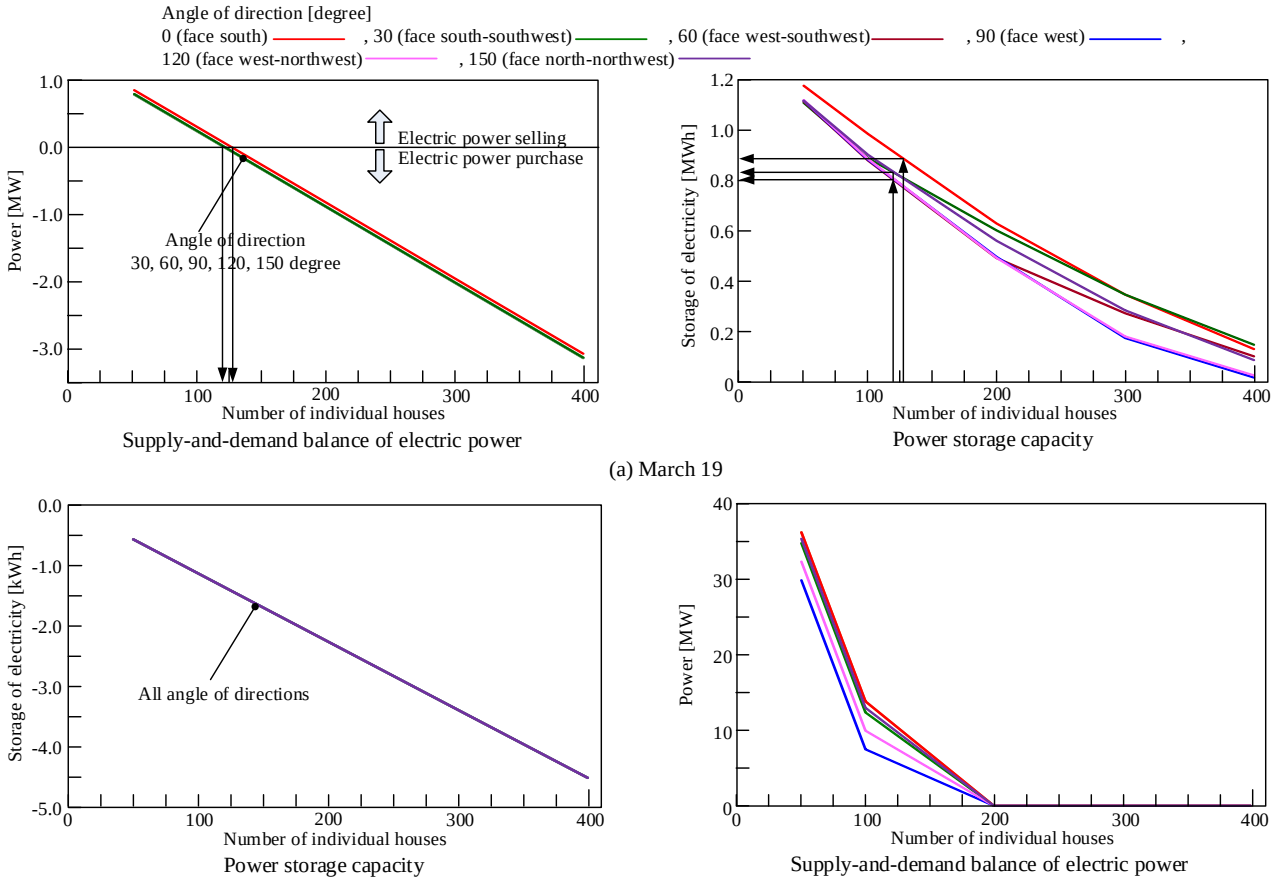

Fig. 15 Supply-and-demand balance of monofacial PV power of 1000 m² based on the supply pattern of the electric power company.

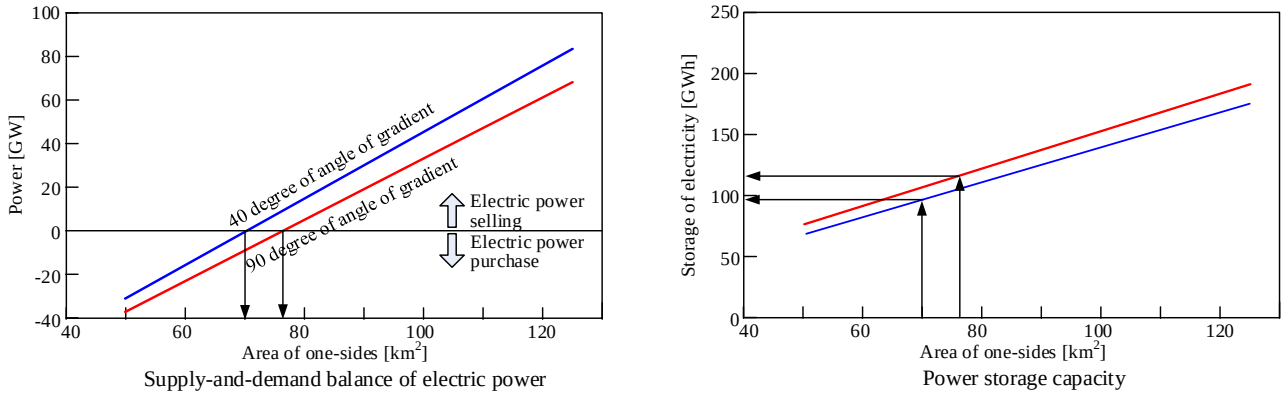

(a) March 19

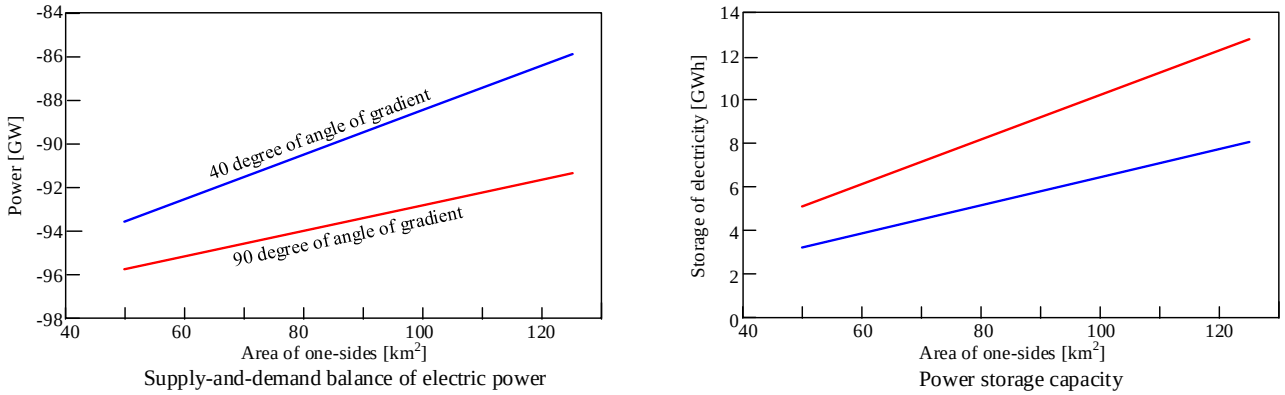

(b) November 26

Fig. 16 Supply-and-demand balance of vertical bifacial PV power of 1000 m² based on the supply pattern of the electric power company.

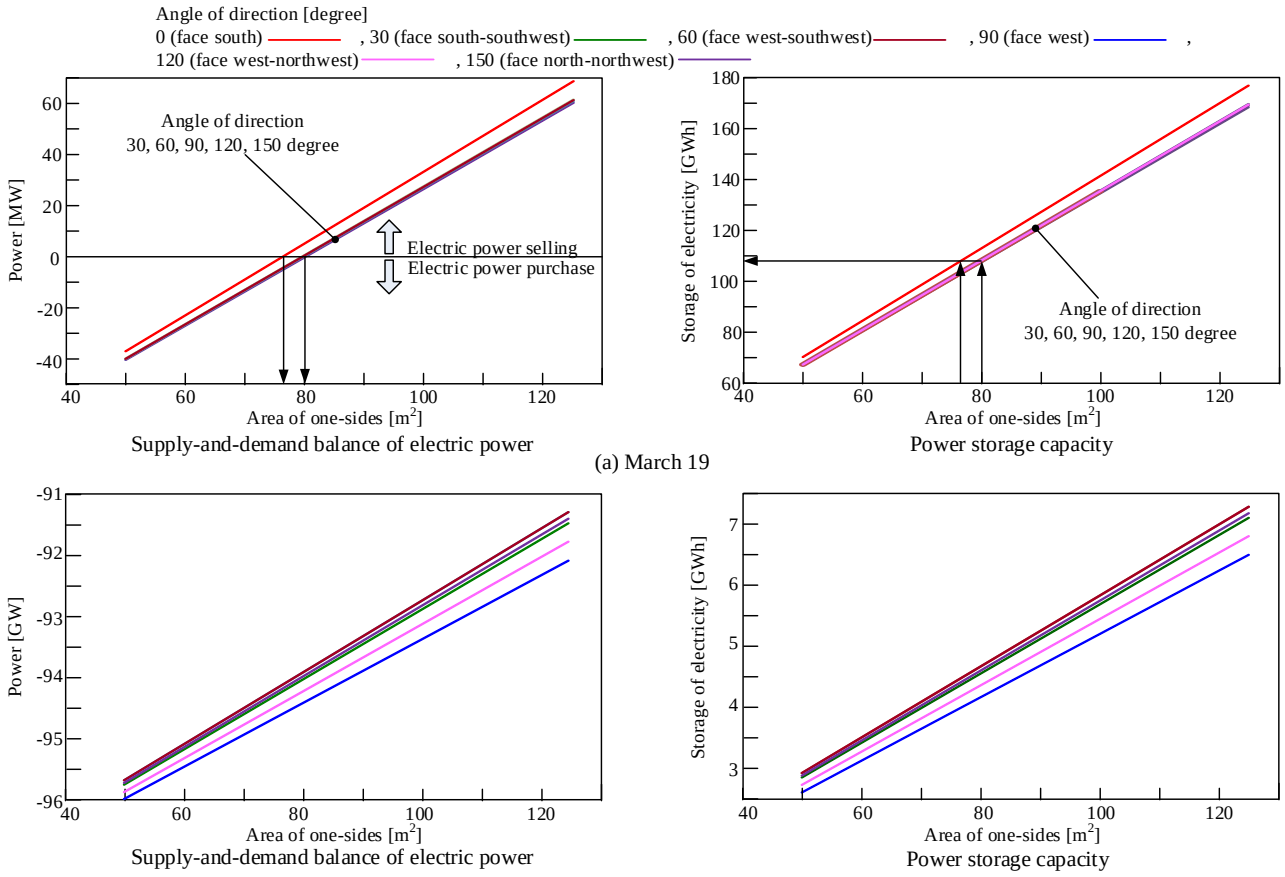

789 Fig. 17 Results of thermal fluid analysis of bifacial PV on August 15 in Kitami (lat. 43°47′ N. and long.
790 143°54′ E).
791
792

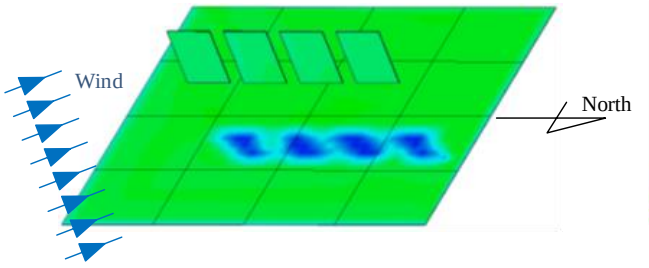

(a) Orientation of 90° (facing east–west), 14:00, wind direction from the southeast of 1 m/s.

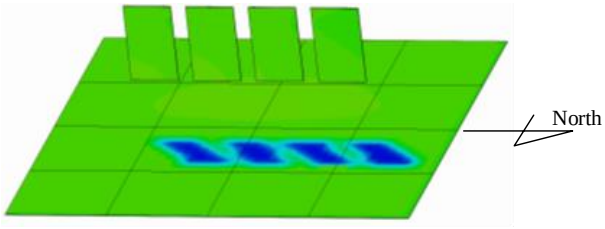

(b) Orientation of 90° (facing east–west), 14:00, no wind.

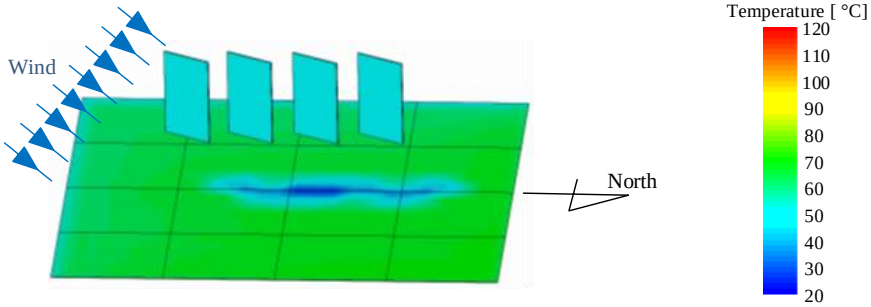

(c) Orientation of 15°, 14:00, wind direction from the southwest of 1 m/s.

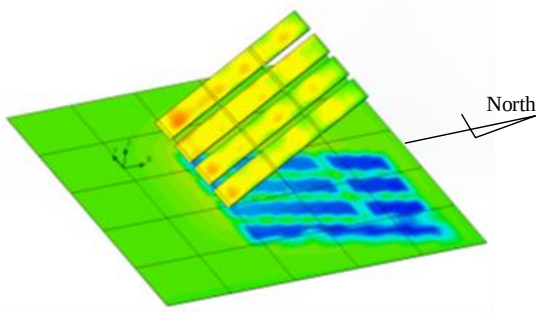

(d) 0.940 m × 1.56 m bifacial modules of 12 sets, orientation of 0° (facing south), 14:00, no wind.

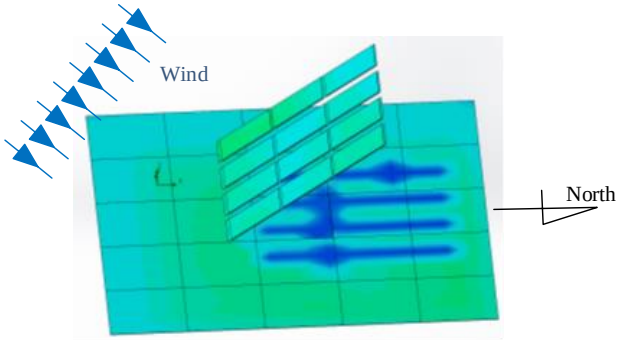

(e) 0.940 m × 1.56 m bifacial modules of 12 sets, the orientation of 0° (facing south), 12:00, wind direction from the southwest of 3 m/s.

(f) Photograph of 0.940 m × 1.56 m bifacial modules of 12 sets, orientation of 0°

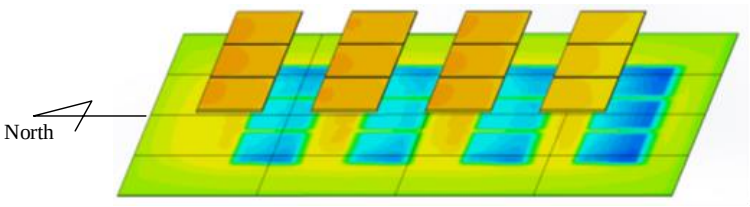

(g) 0.940 m × 1.56 m bifacial modules of 12 sets, horizontal installation, 12:00, no wind.

793